J Nanostruct 16(2): 1721-1732, Spring 2026

RESEARCH PAPER

Modification the Structural and Optical Properties of ZnO:Al Nanoparticles for Enhanced Antibacterial Activity

Vahdat Rafee [1] *, *Alireza Razeghizade* [1], *Safieh Soufian* [2]

[1] *Department of Physics, Faculty of Science, Payame Noor University, Tehran, Iran*
[2] *Department of Biology, Faculty of Science, Payame Noor University, Tehran, Iran*

ARTICLE INFO

Article History:
Received 19 December 2025
Accepted 26 March 2026
Published 01 April 2026

Keywords:
Aluminum
Staphylococcus aureus
Escherichia coli
Microbial resistance
Reactive oxygen species (ROS) generation
Zinc oxide nanoparticles

ABSTRACT

This research involved the synthesis of ZnO:Al nanoparticles with varying doping levels (0%, 4%, 6%, and 8%). Subsequently, a comprehensive analysis was conducted on the samples to evaluate their antibacterial, structural, morphological, and optical characteristics. XRD analysis confirmed a hexagonal Wurtzite structure in all samples, with peak shifts toward higher angles as aluminum doping increased, indicating a reduction in crystallite size. SEM images showed an increase in particle size and improved homogeneity. UV-Vis analysis showed that an increase in aluminum doping led to a rise in the optical band gap from 3.62 eV in pure ZnO to 3.90 eV, suggesting alterations in the material's electronic structure. The antibacterial efficacy of the 8% ZnO:Al nanoparticles was assessed against Staphylococcus aureus and Escherichia coli, revealing that the 8% sample demonstrated the strongest antibacterial properties, with more significant inhibition zones observed for *S. aureus*.

How to cite this article
Rafee V., Razeghizade A., Soufian S. Modification the Structural and Optical Properties of ZnO:Al Nanoparticles for Enhanced Antibacterial Activity. J Nanostruct, 2026; 16(2):1721-1732. DOI: 10.22052/JNS.2026.02.024

INTRODUCTION

ZnO nanoparticles have attracted considerable interest because of their broad band gap (~3.3 eV at ambient temperature) [1-4], remarkable photocatalytic efficiency [5], superior optical characteristics [6], and inherent antibacterial capabilities [7-10]. These characteristics make ZnO nanoparticles highly applicable in biosensors [11-13], optoelectronics [14, 15], environmental catalysts [16, 17], antibacterial coatings [18], and medical technologies [18, 19]. Recent studies have focused on enhancing the properties of ZnO by reducing particle size, altering synthesis techniques, engineering defects, and doping with different metal elements [20-25].

Earlier research has shown that the incorporation of metals like aluminum (Al) [26], gallium (Ga) [27], and indium (In) [28] can significantly enhance its electronic and optical properties. For instance, in several studies, aluminum-doped ZnO (ZnO:Al) has exhibited improved electrical conductivity and reduced resistance to ultraviolet (UV) light [29], making it an ideal candidate for thin-film transistors (TFTs) [30, 31], solar cells [32], and light-emitting diodes (LEDs) [33]. Additionally, other investigations have shown that ZnO:Al nanoparticles serve as highly efficient photocatalysts for environmental pollutant degradation, suggesting their potential role in water and air purification [34].

Nonetheless, accurately controlling doping concentrations and understanding their effects on

* *Corresponding Author Email: V.Rafee@pnu.ac.ir*

the crystal structure, particle size, and both optical and electronic properties of these nanoparticles continues to be a significant challenge. Meanwhile, the worldwide issue of microbial resistance has redirected research efforts toward new avenues in antibacterial materials [35-37]. Multiple studies have shown that ZnO nanoparticles can act as a powerful alternative to conventional antibiotics through cell wall disruption [38], oxidative stress induction, and reactive oxygen species (ROS) generation [39, 40]. Recent findings indicate that the antibacterial activity of ZnO nanoparticles depends on various factors such as particle size [41], doping concentration [42], surface area [41], and interaction with bacterial cells [41]. In some studies, increasing the surface area of ZnO nanoparticles has led to a substantial improvement in antibacterial properties [41]. Additionally, recent research has suggested that doping ZnO with aluminum may enhance its antibacterial activity, but the exact mechanism behind this enhancement remains unclear [43].

In this study, Escherichia coli (*E. coli*) and Staphylococcus aureus (S. aureus) were selected as representative bacterial strains for evaluating the antibacterial efficiency of ZnO:Al nanoparticles. These bacteria were chosen due to their clinical significance and distinct structural differences. *S. aureus*, a Gram-positive pathogen, is known for its thick peptidoglycan layer, making it a major cause of skin infections, pneumonia, and bloodstream infections, often exhibiting antibiotic resistance (e.g., MRSA). *E. coli*, a Gram-negative bacterium, is frequently associated with foodborne illnesses and urinary tract infections (UTIs), characterized by an outer membrane containing lipopolysaccharides (LPS), which can influence the interaction with nanoparticles. By selecting these two bacteria, this study aims to explore how ZnO:Al nanoparticles interact with both Gram-positive and Gram-negative bacterial structures, providing a broader understanding of their antibacterial mechanisms and potential applications in healthcare and environmental disinfection.

This research focused on synthesizing ZnO:Al nanoparticles with varying doping levels (0%, 4%, 6%, and 8%) to systematically examine the influence of doping on their crystal structure, optical characteristics, and antibacterial activity. For this purpose, XRD, SEM, and UV-Vis analyses were conducted to determine the crystal structure, particle size, and optical properties, while their impact on the antibacterial activity against S. aureus and E. coli was assessed using disk diffusion, Minimum Inhibitory Concentration (MIC), and optical density (OD_{600}) reduction tests.

The objective of this study is to develop a better understanding of the relationship between the crystal structure, optical properties, and biological performance of ZnO:Al nanoparticles, paving the way for optimizing these materials for biomedical, optoelectronic, and environmental applications. The results of this research may contribute to the design of highly efficient nanoparticles for combating microbial resistance and enhancing the photocatalytic and optoelectronic performance of ZnO–based materials.

MATERIALS AND METHODS

Experimental Materials and Equipment

Zinc acetate dihydrate [$Zn(CH_3COO)_2{\cdot}2H_2O$], dimethyl sulfoxide (DMSO), aluminum nitrate [$Al(NO_3)_3{\cdot}9H_2O$], sodium carbonate [Na_2CO_3], deionized water, S. aureus (ATCC 25923), E. coli (ATCC 25922), Brain Heart Infusion Broth (BHIB), Brain Heart Infusion Agar (BHIA), Mueller Hinton Broth (MHB), Mueller Hinton Agar (MHA), Nutrient Broth (NB), Nutrient Agar (NA), Resazurin dye (0.02% w/v), X-ray diffraction (XRD) Siemens D5000, scanning electron microscope (SEM) LEO 1455VP, UV–Vis spectrophotometer Perkin Elmer, autoclave, laminar flow hood, spectrophotometer, 96-well microplate, microplate reader, incubator with temperature control at 30°C and 37°C, sonicator, micropipettes with volumes of 50, 100, 200, and 1000 µL, sterile loop, sterile swab.

Experimental Methods

Nanoparticle Synthesis

ZnO:Al nanoparticles with different doping percentages (0%, 4%, 6%, and 8%) were synthesized using zinc acetate dihydrate [$Zn(CH_3COO)_2{\cdot}2H_2O$], aluminum nitrate [$Al(NO_3)_3{\cdot}9H_2O$], and sodium carbonate [Na_2CO_3] as precursors. Initially, a specific amount of zinc acetate was dissolved in 100 mL of ethanol, while aluminum nitrate was dissolved in another beaker containing ethanol as a solvent. The solutions were stirred at 65°C using a magnetic stirrer (Top HS15 model M) for 20 minutes until a clear solution was obtained. Then, the sodium carbonate solution was gradually added to the mixture and stirred for 1 hour. The final product was calcined at 500°C, resulting in ZnO:Al nanoparticles with varying aluminum content [44].

The synthesized nanoparticles were characterized using X-ray diffraction (XRD) for crystal structure analysis, scanning electron microscopy (SEM) for morphology and particle size determination, and UV–Vis spectrophotometry for optical property evaluation. Before conducting antibacterial tests, the nanoparticles were suspended in dimethyl sulfoxide DMSO and sonicated for 20 minutes to ensure uniform dispersion.

Antibacterial Testing

The antibacterial activity of ZnO:Al nanoparticles was assessed against E. coli (ATCC 25922) and S. aureus (ATCC 25923) through disk diffusion, MIC, Minimum Bactericidal Concentration (MBC) and optical density (OD_{600}) measurements. Mueller Hinton Agar (MHA) plates were prepared for the disk diffusion assay, with bacterial strains evenly spread across the surface. Sterile disks loaded with nanoparticle solutions at concentrations of 0.01%, 0.5%, and 1% were placed onto the agar, and the plates were incubated at 37°C for 24 hours. The inhibition zone diameter was measured to assess bacterial susceptibility. For the MIC test, wells of a 96-well microplate from columns 1 to 10 were filled with 50 µL of BHI broth, followed by the addition of 50 µL of sonicated nanoparticles to the first column and serial two-fold dilutions across the plate. Subsequently, 50 µL of bacterial inoculum (10^6 CFU/mL) was added to each well,

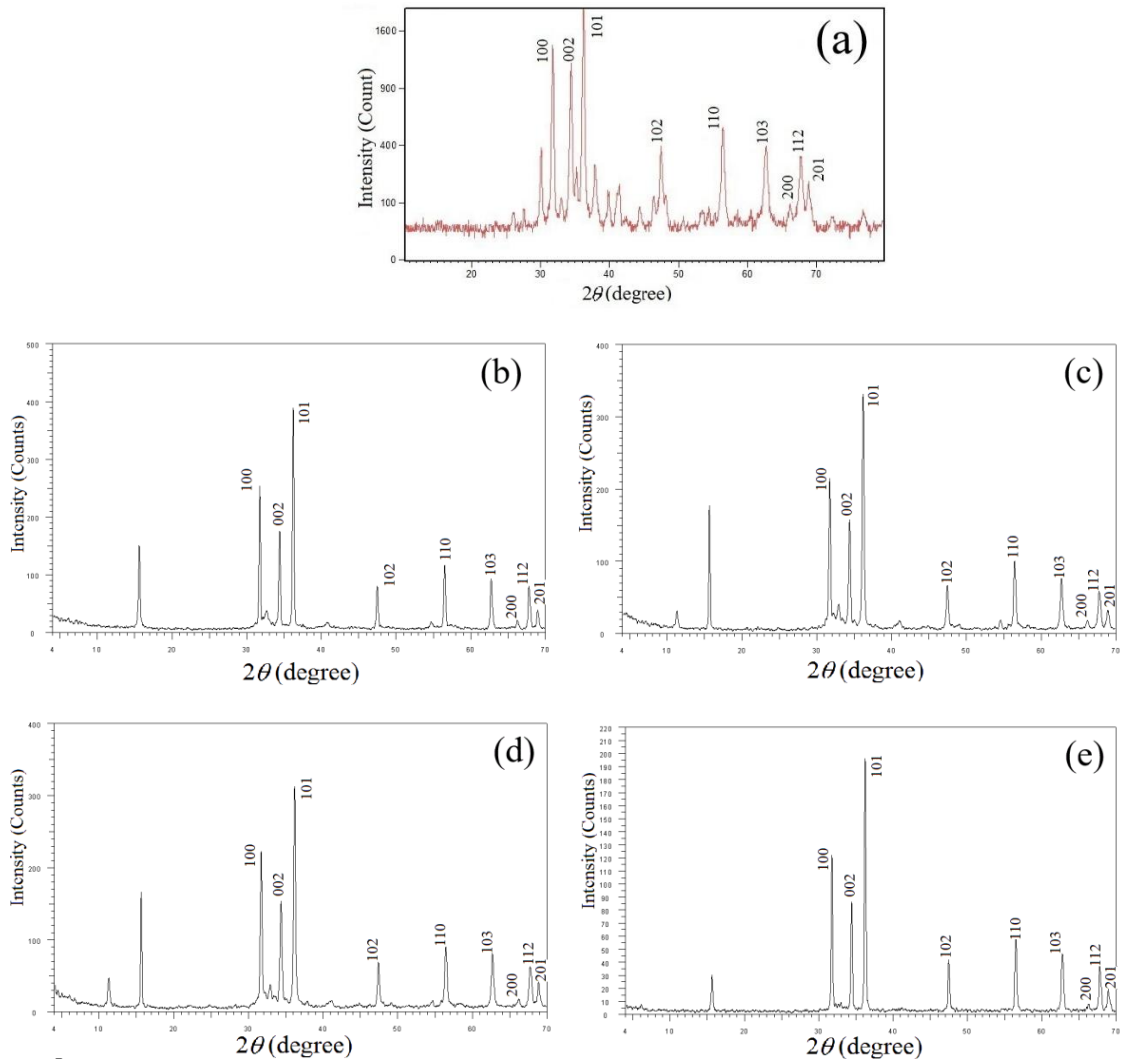

Fig. 1. XRD results for nanoparticles: (a) pure ZnO and Al-doped ZnO with doping levels of (b) 2%, (c) 4%, (d) 6%, and (e) 8% aluminum.

while positive control (column 11, containing bacteria only) and sterility control (column 12, containing **only** BHI broth**)** were included. The microplate was incubated at **37°**C for 24 hours, followed by the addition of 20 µL of Resazurin dye (0.02% w/v) to each well and further incubation for 2 hours [45, 46**]**. The last well that remained blue was recorded as the MIC value. To examine bacterial growth in a liquid medium, 2 mL of overnight bacterial culture of *S. aureus* and *E. coli* was inoculated into 100 mL of nutrient broth (NB) + 0.12% glucose**,** with four groups including control (without nanoparticles), 0.01%, 0.5%, and 1% nanoparticle concentrations**.** The samples were incubated at 30°C for 24 hours, and bacterial growth was assessed by measuring optical density at 600 nm (OD_{600}) using a spectrophotometer [47]**.**

RESULTS AND DISCUSSION

Structural and Morphological Analysis of Nanoparticles

X-ray Diffraction (XRD) Results

To investigate the structural properties of the synthesized nanoparticles**,** X-ray diffraction (XRD) analysis using the Siemens D5000 device was performed. The XRD patterns were recorded in the 2θ range from 20° to 80° with a step size of 0.02**°** to obtain precise information on the crystalline structure of the nanoparticles [48].

The XRD patterns (Fig. 1) confirm the hexagonal (Wurtzite) structure in all samples (pure ZnO and ZnO doped with 2%, 4%, 6%, and 8% aluminum). These results indicate that the aluminum doping process has not induced any phase transition, and the Wurtzite structure remains stable.

In all samples, the most intense diffraction peak corresponds to the (101) plane, indicating the preferred orientation of the crystallites. A comparison of the diffraction patterns shows that as the aluminum content increases; the diffraction peaks shift toward higher angles**.** This shift can be attributed to the substitution of aluminum ions (with an ionic radius of 0.53Å) for instead of zinc ions (with an ionic radius of 0.60Å) in the ZnO crystalline structure**.** This substitution leads to a contraction of the crystal lattice, reducing the lattice parameters and consequently shifting the diffraction peaks to higher angles (increase in 2θ).

Calculation of Crystallite Size

The average crystallite size was determined using the Debye-Scherrer equation [49]:

$$D=0.94\lambda/\beta\cos\theta \quad (1)$$

Where D, K, λ, β, and θ are the crystallite size (nm), the Scherrer constant (approximately 0.9), the X-ray wavelength (1.54 Å for Cu–Kα), the full width at half maximum (FWHM) of the diffraction peak, and the diffraction angle respectively.

The calculated results are presented in Table 1, showing that as the aluminum concentration increases, the crystallite size decreases**.** This reduction capeakn be attributed to increased lattice strain, the introduction of crystal defects, and restricted crystallite growth due to aluminum

Table 1. Average crystallite size of Al-doped ZnO samples with different aluminum doping percentages.

Sample	Crystallite Size (nm)	(101) Peak Angle (°)	FWHM
ZnO (pure)	28.28	36.24	0.300
$Zn_{0.98}Al_{0.02}O$	25.24	36.21	0.360
$Zn_{0.96}Al_{0.04}O$	15.45	36.19	0.571
$Zn_{0.94}Al_{0.06}O$	14.40	36.16	0.606
$Zn_{0.92}Al_{0.08}O$	12.26	36.20	0.712

Table 2. Average nanoparticle size of Al-doped ZnO samples with different aluminum doping percentages.

Aluminum Percentage (%)	Average Nanoparticle Size (nm)
2%	30
4%	50
6%	54
8%	73

doping**.** Furthermore, the increase in FWHM for samples with higher aluminum content confirms this size reduction.

The results in Table 1 indicate that in the sample with 8% aluminum, the crystallite size reaches its minimum value**.** This reduction can be attributed to the incorporation of aluminum into the ZnO structure, increasing lattice strain and consequently reducing crystallite size.

Scanning Electron Microscope (SEM) Analysis

To study the surface morphology, particle dimensions, and size distribution of nanoparticles, scanning electron microscopy (SEM) using the LEO 1455VP device was performed. SEM images clearly show that increasing the aluminum content leads to an increase in the average nanoparticle size. Furthermore, in samples with higher aluminum concentrations, the nanoparticles exhibit a more uniform distribution and increased adhesion between particles.

The analysis of Fig. 2 and the results of Table 2 indicate that, with an increase in the percentage of aluminum nanoparticles, the particle size has increased, and samples with higher Al content (6% and 8%) exhibit larger particles and greater agglomeration, whereas samples with lower Al content (2% and 4%) have smaller particles with a more uniform distribution. The 2% Al (98% ZnO) sample has the smallest particle size and a more homogeneous distribution, while the 8% Al (92% ZnO) sample has the largest particle size and higher agglomeration. This trend indicates that increasing the amount of aluminum nanoparticles leads to an increase in particle size and agglomeration.

As the aluminum percentage increases, particle growth becomes more pronounced, and aluminum appears to promote ZnO particle aggregation. Samples with lower Al content (2% and 4%) likely have a higher specific surface area, making them more suitable for catalytic or sensing applications. The increase in aluminum content may reduce the effective surface area and lead to an increase in ZnO cluster size. In electronic

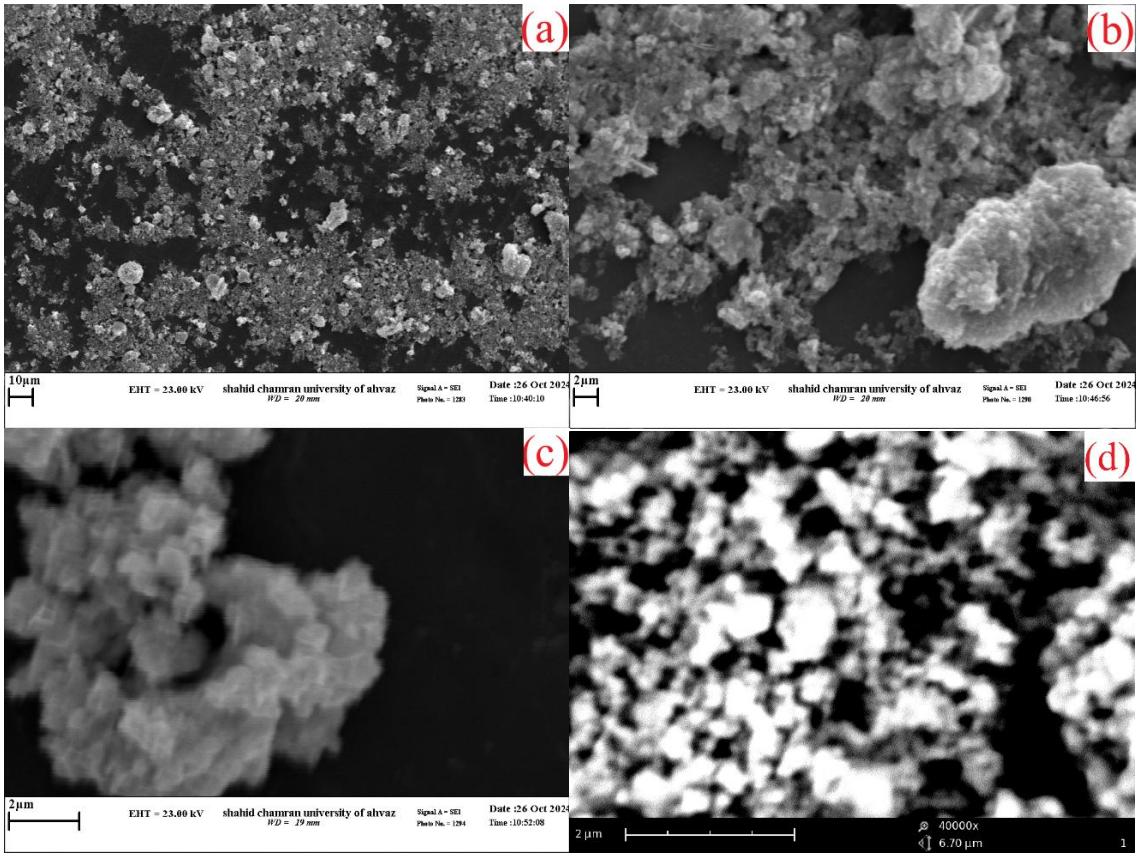

Fig. 2. SEM images of Al-doped ZnO nanoparticles with different doping levels: (a) 8% Al, (b) 6% Al, (c) 4% Al, and (d) 2% Al.

and catalytic applications, samples with lower Al content (such as 2% and 4%) may exhibit better performance due to their higher specific surface area. Therefore, the increase in aluminum has led to an increase in structural defects and interparticle forces, resulting in enhanced agglomeration and, consequently, the growth of nanoparticle size observed in SEM.

Optical Properties Analysis of Nanoparticles

UV–Vis Spectroscopy Analysis

To study the optical properties of nanoparticles, a UV–Vis spectrophotometer (Perkin Elmer) was used. The absorption spectra of the samples were recorded in the 200–800 nm range to investigate electronic transitions and the effect of aluminum doping on the optical properties of the nanoparticles.

Fig. 3 shows the absorption spectra of pure ZnO nanoparticles and ZnO doped with 2%, 4%, 6%, and 8% aluminum. The absorption peak of pure ZnO is observed at approximately 370 nm, which is consistent with previous reports on the ZnO band gap. In the doped samples, as the aluminum percentage increases, the absorption peak shifts toward shorter wavelengths (blue shift), indicating an increase in the band gap energy.

This shift in the absorption peak position can be attributed to several factors, including the increase in nanoparticle size due to aluminum doping, which enhances quantum confinement effects and increases the band gap energy, as well as the Burstein–Moss effect, where an increase in the concentration of free charge carriers results in the filling of lower energy states in the conduction band, causing an apparent increase in the optical band gap.

Band Gap Energy Calculation

To determine the band gap energy of the nanoparticles, the Tauc plot method was used. The equation applied is as follows [50]:

$$\alpha h\upsilon = (h\upsilon - Eg)^n \quad (2)$$

Where α, hν, A, E_g and n are the absorption coefficient, the photon energy, a constant, the optical band gap energy, a parameter dependent on the nature of the electronic transitions, which is 2 for direct allowed transitions in semiconductors.

To accurately determine the band gap energy, a plot of $(\alpha h\nu)^2$ versus hν was created, and the extrapolated intercept of the linear region with the x-axis was taken as the optical band gap energy.

The results of Table 3 indicate that as the aluminum doping percentage increases, the band gap energy increases. This increase can be attributed to lattice defects, increases in

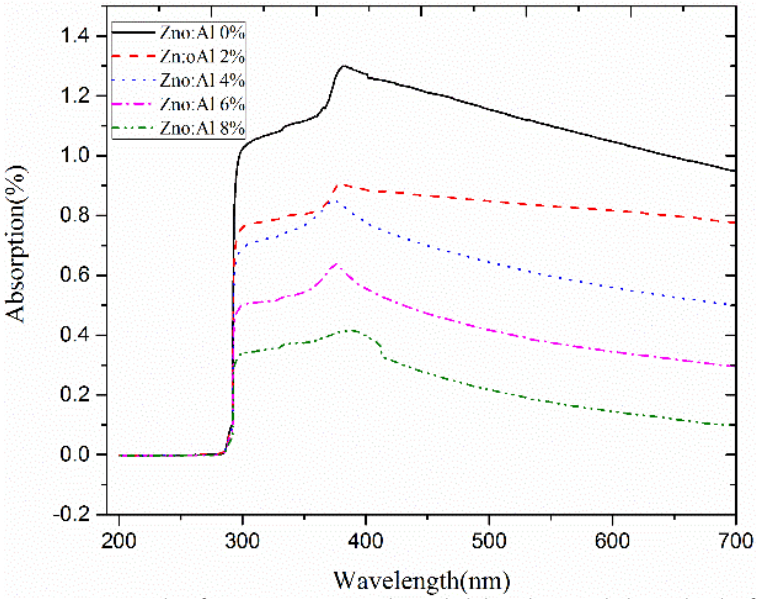

Fig. 3. UV–Vis results of pure ZnO nanoparticles and Al-doped ZnO with doping levels of 2%, 4%, 6%, and 8% aluminum.

nanoparticle size, and quantum confinement effects. Additionally, a significant amount of aluminum might introduce extra energy states in the conduction band, influencing the optical band gap.

Absorption Intensity Analysis and Doping Effects

As observed in the absorption spectra, the absorption intensity of doped samples is lower compared to pure ZnO. This reduction in absorption intensity can be attributed to increased light scattering, a decrease in electronic state density, and changes in the band structure due to doping. In the 8% aluminum-doped sample, the lowest absorption intensity is recorded, suggesting that excessive doping may reduce the optical efficiency of the nanoparticles. The shift of the absorption peak toward shorter wavelengths (blue shift) due to aluminum doping further confirms the direct influence of doping on the electronic structure of ZnO nanoparticles.

Antibacterial Properties Analysis of Nanoparticles
Evaluation of Antimicrobial Effects of Nanoparticles

To study the antibacterial effects of the synthesized nanoparticles, biological assays were performed using *S. aureus* (ATCC 25923) and Escherichia coli. The impact of nanoparticles on bacterial growth was evaluated using bacterial growth assessment in liquid medium, determination of Minimum Inhibitory Concentration (MIC), and determination of MBC. Nanoparticle samples were suspended in Dimethyl sulfoxide (DMSO) and sonicated for 20 minutes for uniform dispersion.

Bacterial Growth Evaluation in the Presence of Nanoparticles

In this experiment, the effect of different nanoparticle concentrations on the growth of S. aureus and *E. coli* was analyzed in Nutrient Broth (NB) and Brain-Heart Infusion Broth (BHIB). For each test, 2 mL of overnight bacterial culture was added to 100 mL of culture medium containing nanoparticles at concentrations of 0.01%, 0.5%, and 1%, followed by incubation at 30°C for 24 hours. The results showed that a 0.01% nanoparticle concentration had no significant effect on bacterial growth, while a 0.5% concentration reduced the optical density (OD) of the bacterial solution by 1.9 times compared to the control ($p<0.05$). Additionally, a 1% concentration caused a 4.5-fold OD reduction in *S. aureus* cultures and a 3.3-fold reduction in *E. coli* cultures relative to the control group. These findings indicate that higher nanoparticle concentrations exhibit greater inhibitory effects on bacterial growth, with 8% aluminum-doped nanoparticles demonstrating the strongest antimicrobial effect.

Determination of Minimum Inhibitory Concentration (MIC)

The MIC of nanoparticles was determined using the serial dilution method in a 96-well plate according to the CLSI M07-A10 protocol. The procedure involved adding 50 µL of Brain-Heart Infusion Broth (BHI) to wells in columns 1 to 10, performing twofold serial dilutions of

Table 3. The calculated band gap values.

Aluminum Percentage (%)	Band Gap (eV)
0% (Pure ZnO)	3.62
2%	3.65
4%	3.75
6%	3.88
8%	3.90

Table 4. Presents the MIC values of the nanoparticles.

Sample	S. aureus (µg/mL)	E. coli (µg/mL)
ZnO (Pure)	250	500
$Zn_{0.98}Al_{0.02}O$	150	320
$Zn_{0.96}Al_{0.04}O$	90	200
$Zn_{0.94}Al_{0.06}O$	50	120
$Zn_{0.92}Al_{0.08}O$	25	80

nanoparticles in the respective wells, adding 50 µL of *S. aureus* culture to each well, using column 11 as a positive bacterial growth control, and column 12 as a sterile (bacteria-free) control. After 24 hours of incubation at 37°C, 20 µL of Resazurin dye (0.02% w/v) was added to each well, followed by an additional 2-hour incubation. The MIC results of Table 4 showed that nanoparticles with 8% aluminum had the lowest MIC value for *S. aureus*, antibacterial activity was stronger against *S. aureus* than *E. coli*, indicating a higher efficacy against Gram-positive bacteria, and the MIC of 8% aluminum-doped nanoparticles was approximately 10 times lower than that of pure ZnO nanoparticles.

Determination of Minimum Bactericidal Concentration (MBC)

After determining the MIC, the MBC was also evaluated. For this purpose, 10 µL from wells containing MIC and higher concentrations were plated on Brain-Heart Infusion Agar (BHA) and incubated at 37°C for 24 hours.

Table 5 presents the MBC values of ZnO:Al nanoparticles for *E. coli* and *S. aureus*. The results indicate that nanoparticles with 8% aluminum doping exhibit the lowest MBC values (50 µg/mL for *S. aureus* and 168 µg/mL for *E. coli*), highlighting their strong bactericidal effect. In contrast, pure ZnO shows the highest MBC values (4125 µg/mL for *S. aureus* and 8500 µg/mL for *E. coli*), indicating a weak antimicrobial effect. Additionally, MBC values for *E. coli* are consistently higher than those for *S. aureus*, which aligns with the greater resistance of Gram-negative bacteria due to their outer membrane. These findings underscore the role of aluminum doping in enhancing the antibacterial efficacy of ZnO nanoparticles.

Table 6 displays the MBC/MIC ratios of ZnO:Al nanoparticles for *S. aureus* and *E. coli*. The ratios for *E. coli* are approximately 3% higher than those for *S. aureus*, reflecting the greater resistance of Gram-negative bacteria due to their outer membrane. Notably, the 8% aluminum-doped nanoparticles exhibit the lowest ratios (2 for *S. aureus* and 1.9 for *E. coli*), indicating a strong bactericidal effect, while pure ZnO shows the highest ratios (16.5 for *S. aureus* and 15.0 for *E. coli*), suggesting a predominantly bacteriostatic effect. These findings highlight the enhanced antibacterial potency with increasing aluminum doping.

Additionally, in Fig. 4, Fig. 5 and Table 7, the labels are specified as follows: 1 = 0.01%, 2 = 0.5%, 3 = 1%, 4 = DMSO, and 5 = Blank disc.

Analysis of Zone of Inhibition Measurements

In this study, the effect of ZnO:Al nanoparticles with different aluminum doping percentages on the growth of *S. aureus* and *E. coli* was

Table 5. Presents the MBC values of the nanoparticles.

Sample	S. aureus (µg/mL)	E. coli (µg/mL
ZnO (Pure)	4125	8500
$Zn_{0.98}Al_{0.02}O$	900	1984
$Zn_{0.96}Al_{0.04}O$	720	1640
$Zn_{0.94}Al_{0.06}O$	600	1488
$Zn_{0.92}Al_{0.08}O$	50	168

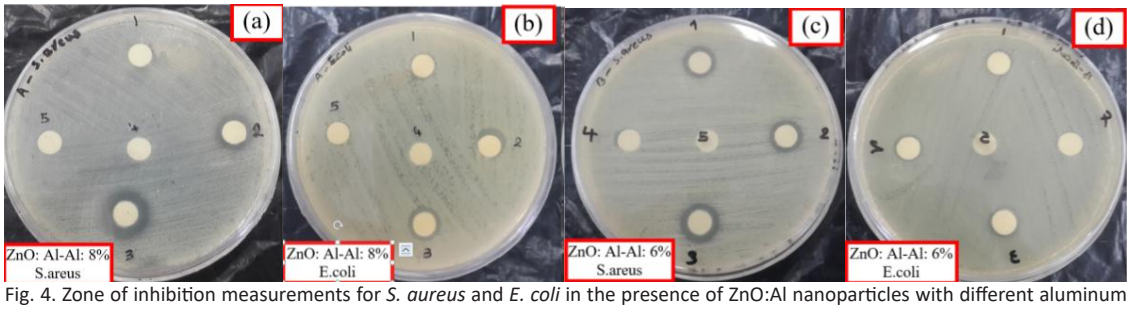

Fig. 4. Zone of inhibition measurements for *S. aureus* and *E. coli* in the presence of ZnO:Al nanoparticles with different aluminum doping percentages at various nanoparticle concentrations (0.01%, 0.5%, 1% and Control groups include DMSO and a blank disc).

investigated. For this purpose, the zone of inhibition measurements were carried out in the presence of ZnO:Al nanoparticles with various aluminum doping percentages (0%, 4%, 6%, and 8%) at different nanoparticle concentrations (0.01%, 0.5%, and 1%). These measurements are presented in Table 7, which shows the zone of inhibition for each aluminum doping percentage at different nanoparticle concentrations.

The results showed that ZnO:Al nanoparticles with 8% aluminum doping had the highest effect on inhibiting the growth of *S. aureus*, with the zone of inhibition reaching 15 mm at the 1% concentration (as seen in Fig. 4, which presents the inhibition zones in the presence of ZnO:Al nanoparticles). In contrast, the effect of nanoparticles on *E. coli* was weaker, with the maximum zone of inhibition reaching 11 mm.

Additionally, the results in the graphs of Fig. 5 demonstrated that as the aluminum doping percentage increased, the antibacterial effect of ZnO:Al nanoparticles also improved, especially against *S. aureus*. Nanoparticles with 4% aluminum doping and without aluminum doping

Table 6. MBC/MIC Ratios for ZnO:Al Nanoparticles.

Sample	S. aureus	E. coli
ZnO (Pure)	16.5	15.0
$Zn_{0.98}Al_{0.02}O$	6	5.8
$Zn_{0.96}Al_{0.04}O$	8	7.6
$Zn_{0.94}Al_{0.06}O$	12	11.8
$Zn_{0.92}Al_{0.08}O$	2	1.9

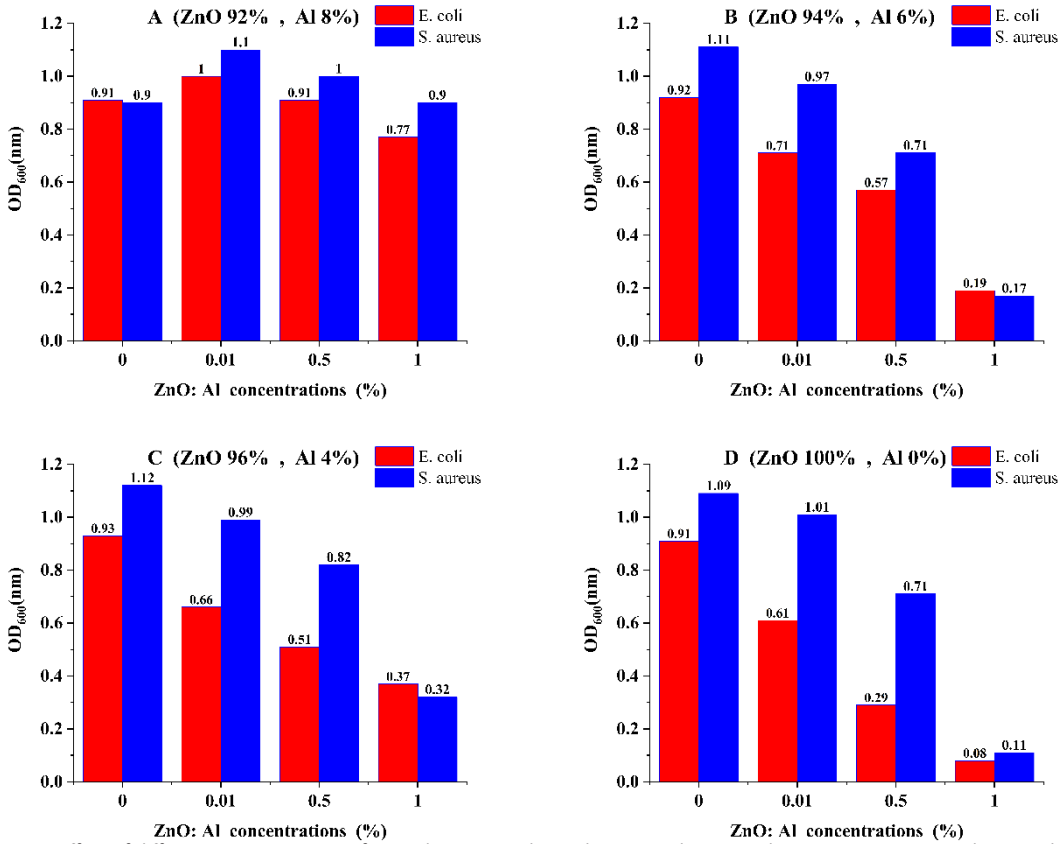

Fig. 5. Effect of different concentrations of ZnO:Al nanoparticles with various aluminum doping percentages on the growth of *S. aureus* and *E. coli*.

Table 7. Zone of inhibition measurements for *S. aureus* and *E. coli* in the presence of ZnO:Al nanoparticles with different aluminum doping percentages at various nanoparticle concentrations (0.01%, 0.5%, 1% and Control groups include DMSO and a blank disc).

nanoparticles	Organism	Zone of Inhibition (mm) (Diameter)				
		1	2	3	4	5
A=8% AL	S. aureus	10	12	15	0	0
	E. coli	8	10	11	0	0
B= 6% AL	S. aureus	11	11	12	0	0
	E. coli	9	9	9	0	0
C=4% AL	S. aureus	1	12	13	0	0
	E. coli	9	11	9	0	0
D=0% AL	S. aureus	0	9	11	0	0
	E. coli	0	0	0	0	0

(0%) showed weaker effects in inhibiting bacterial growth. Increasing the nanoparticle concentration also positively influenced the growth inhibition zone for *S. aureus*.

In conclusion, these results indicate that ZnO:Al nanoparticles with different aluminum doping percentages can effectively inhibit the growth of certain bacteria, especially *S. aureus*. Therefore, these nanoparticles could have potential applications in antibacterial and medical fields, particularly in combating infections caused by *S. aureus*.

Possible Mechanism of Antibacterial Activity of Nanoparticles

The antibacterial activity of ZnO:Al nanoparticles can be attributed to several mechanisms, including the generation of ROS, where ZnO and aluminum-doped nanoparticles produce ROS that cause membrane damage and bacterial cell destruction. Another mechanism is the electrostatic interaction with the bacterial membrane, as ZnO nanoparticles carry a positive charge, allowing them to interact with the negatively charged bacterial membrane and disrupt its permeability [9].

Additionally, disruption of membrane proteins occurs when ZnO nanoparticles interact with thiol (-SH) groups of membrane proteins, altering their function and ultimately leading to cell death. Furthermore, biofilm inhibition and reduced cell adhesion play a role, as nanoparticles may prevent bacterial biofilm formation, thereby inhibiting bacterial attachment and colonization on surfaces.

CONCLUSION

This study demonstrated that aluminum doping significantly affects the physical properties and antibacterial performance of ZnO nanoparticles. Structurally, aluminum incorporation into the ZnO crystal lattice reduced crystallite size, shifted XRD diffraction peaks, and improved particle homogeneity. In terms of optical properties, the increase in the optical band gap and the blue shift in absorption confirmed the modifications in ZnO's electronic structure, enhancing its efficiency for photonic and catalytic applications.

Antibacterial assessments revealed that 8% ZnO:Al exhibited the highest inhibitory effect on bacterial growth, with *S. aureus* being more sensitive to the nanoparticles than *E. coli*. This difference is likely due to variations in the bacterial cell wall structures and stronger electrostatic interactions between the nanoparticles and *S. aureus*.

Given these findings, ZnO:Al nanoparticles hold great potential for optoelectronic devices, antibacterial coatings, biosensors, and biomedical applications. Further studies on their thermal stability, electrical behavior, and cytotoxicity are recommended to optimize their industrial and biomedical applications.

CONFLICT OF INTEREST

The authors declare that there is no conflict of interests regarding the publication of this manuscript.

REFERENCE

1. Özgür Ü, Alivov YI, Liu C, Teke A, Reshchikov MA, Doğan S, et al. A comprehensive review of ZnO materials and devices. J Appl Phys. 2005;98(4).
2. Rafee V, Razaghizadeh A, Nakhaei R, Hosini R. Eco-friendly dye-sensitized solar cells: Green synthesis of ZnO nanoparticles using Sargassum algae and performance enhancement through optimized dye combinations.

Materials Science and Engineering: B. 2025;317:118164.
3. Rafee V, Razeghizadeh A, Yazdizadeh F, Nakhaei R. Efficiency enhancement of DSSCs based on sol-gel prepared ZnO nanoparticles through cosensitization with natural and synthetic pigments. Chemical Physics Impact. 2025;10:100868.
4. Biswas R, Chatterjee S. Effect of surface modification via sol-gel spin coating of ZnO nanoparticles on the performance of WO_3 photoanode based dye sensitized solar cells. Optik. 2020;212:164142.
5. Mu J, Shao C, Guo Z, Zhang Z, Zhang M, Zhang P, et al. High Photocatalytic Activity of ZnO–Carbon Nanofiber Heteroarchitectures. ACS Applied Materials and Interfaces. 2011;3(2):590-596.
6. Pratomo U, Fransisca N, Adzani MD, Irkham I, Sulaeman AP, Eddy DR, et al. Doping of rare earth element: The effects in elevated physical and optical properties of ZnO. Talanta Open. 2025;11:100411.
7. Sedefoglu N, Veryer K, Zalaoglu D, Bozok F. Antibacterial and photocatalytic performances of bioactive In-doped ZnO nanoparticles. Materials Science and Engineering: B. 2025;313:117914.
8. Liu J, Wang Y, Ma J, Peng Y, Wang A. A review on bidirectional analogies between the photocatalysis and antibacterial properties of ZnO. J Alloys Compd. 2019;783:898-918.
9. Sirelkhatim A, Mahmud S, Seeni A, Kaus NHM, Ann LC, Bakhori SKM, et al. Review on Zinc Oxide Nanoparticles: Antibacterial Activity and Toxicity Mechanism. Nano-Micro Letters. 2015;7(3):219-242.
10. Sharma DK, Shukla S, Sharma KK, Kumar V. A review on ZnO: Fundamental properties and applications. Materials Today: Proceedings. 2022;49:3028-3035.
11. Tereshchenko A, Bechelany M, Viter R, Khranovskyy V, Smyntyna V, Starodub N, et al. Optical biosensors based on ZnO nanostructures: advantages and perspectives. A review. Sensors Actuators B: Chem. 2016;229:664-677.
12. Krishna MS, Singh S, Batool M, Fahmy HM, Seku K, Shalan AE, et al. A review on 2D-ZnO nanostructure based biosensors: from materials to devices. Materials Advances. 2023;4(2):320-354.
13. Eveness J, Cao L, Kiely J, Luxton R. Equivalent circuit model of a non-faradaic impedimetric ZnO nano-crystal biosensor. J Electroanal Chem. 2022;906:116003.
14. Shahzad S, Javed S, Usman M. A Review on Synthesis and Optoelectronic Applications of Nanostructured ZnO. Frontiers in Materials. 2021;8.
15. Djurišić AB, Ng AMC, Chen XY. ZnO nanostructures for optoelectronics: Material properties and device applications. Progress in Quantum Electronics. 2010;34(4):191-259.
16. Sun Y, Chen L, Bao Y, Zhang Y, Wang J, Fu M, et al. The Applications of Morphology Controlled ZnO in Catalysis. Catalysts. 2016;6(12):188.
17. Baig A, Siddique M, Panchal S. A Review of Visible-Light-Active Zinc Oxide Photocatalysts for Environmental Application. Catalysts. 2025;15(2):100.
18. Puspasari V, Ridhova A, Hermawan A, Amal MI, Khan MM. ZnO-based antimicrobial coatings for biomedical applications. Bioprocess and Biosystems Engineering. 2022;45(9):1421-1445.
19. Medina Cruz D, Mostafavi E, Vernet-Crua A, Barabadi H, Shah V, Cholula-Díaz JL, et al. Green nanotechnology-based zinc oxide (ZnO) nanomaterials for biomedical applications: a review. Journal of Physics: Materials. 2020;3(3):034005.
20. Dao DV, van den Bremt M, Koeller Z, Le TK. Effect of metal ion doping on the optical properties and the deactivation of photocatalytic activity of ZnO nanopowder for application in sunscreens. Powder Technol. 2016;288:366-370.
21. Schumann J, Lunkenbein T, Tarasov A, Thomas N, Schlögl R, Behrens M. Synthesis and Characterisation of a Highly Active Cu/ZnO:Al Catalyst. ChemCatChem. 2014;6(10):2889-2897.
22. Kshirsagar SD, Shelake SP, Biswas B, Ramesh K, Gaur R, Abraham BM, et al. Emerging ZnO Semiconductors for Photocatalytic CO2 Reduction to Methanol. Small. 2024;20(50).
23. Divband B, Khatamian M, Eslamian GRK, Darbandi M. Synthesis of Ag/ZnO nanostructures by different methods and investigation of their photocatalytic efficiency for 4-nitrophenol degradation. Appl Surf Sci. 2013;284:80-86.
24. Jayakumar OD, Persson C, Tyagi AK, Sudakar C. Experimental and Theoretical Investigations of Dopant, Defect, and Morphology Control on the Magnetic and Optical Properties of Transition Metal Doped ZnO Nanoparticles. Springer Series in Materials Science: Springer India; 2013. p. 341-370.
25. Zheng S, Chen Z, Duley WW, Wu YA, Peng P, Zhou YN. Engineering the defect distribution in ZnO nanorods through laser irradiation. Nanotechnology. 2023;34(49):495703.
26. Azizah Nm, Muhammady S, Purbayanto MAK, Nurfani E, Winata T, Sustini E, et al. Influence of Al doping on the crystal structure, optical properties, and photodetecting performance of ZnO film. Progress in Natural Science: Materials International. 2020;30(1):28-34.
27. Schumann J, Eichelbaum M, Lunkenbein T, Thomas N, Álvarez Galván MC, Schlögl R, et al. Promoting Strong Metal Support Interaction: Doping ZnO for Enhanced Activity of Cu/ZnO:M (M = Al, Ga, Mg) Catalysts. ACS Catalysis. 2015;5(6):3260-3270.
28. Hjiri M, Dhahri R, Omri K, El Mir L, Leonardi SG, Donato N, et al. Effect of indium doping on ZnO based-gas sensor for CO. Mater Sci Semicond Process. 2014;27:319-325.
29. Kumar M, Basu T, Som T. Ultra-violet absorption induced modifications in bulk and nanoscale electrical transport properties of Al-doped ZnO thin films. J Appl Phys. 2015;118(5).
30. Li Y, Yao R, Wang H, Wu X, Wu J, Wu X, et al. Enhanced Performance in Al-Doped ZnO Based Transparent Flexible Transparent Thin-Film Transistors Due to Oxygen Vacancy in ZnO Film with Zn–Al–O Interfaces Fabricated by Atomic Layer Deposition. ACS Applied Materials and Interfaces. 2017;9(13):11711-11720.
31. Kim SY, Kim K, Kim AR, Lee HI, Lee Y, Kim SM, et al. Operation Principles of ZnO/Al_2O_3-AlDMP/ZnO Stacked-Channel Ternary Thin-Film Transistor. Advanced Electronic Materials. 2021;7(6).
32. Song D, Aberle AG, Xia J. Optimisation of ZnO:Al films by change of sputter gas pressure for solar cell application. Appl Surf Sci. 2002;195(1-4):291-296.
33. Sandeep KM, Bhat S, Dharmaprakash SM. Structural, optical, and LED characteristics of ZnO and Al doped ZnO thin films. Journal of Physics and Chemistry of Solids. 2017;104:36-44.
34. Gu X, Li C, Yuan S, Ma M, Qiang Y, Zhu J. ZnO based heterojunctions and their application in environmental photocatalysis. Nanotechnology. 2016;27(40):402001.
35. Mobarki N, Almerabi B, Hattan A. Antibiotic Resistance

Crisis. International Journal of Medicine in Developing Countries. 2019:561-564.
36. Aslam B, Wang W, Arshad MI, Khurshid M, Muzammil S, Rasool MH, et al. Antibiotic resistance: a rundown of a global crisis. Infection and Drug Resistance. 2018;Volume 11:1645-1658.
37. Zainab JM, Sahira K, Al-Abboodi AK, Alsaady HA. Enhancing Pediculicidal Activity Against Pediculus humanus capitis Using Iron Oxide Nanoparticle-Based Formulations of some Plant Extracts and Acetic Acid Solution. Nigerian Journal of Parasitology. 2024;45(2):460-469.
38. Kumar R, Umar A, Kumar G, Nalwa HS. Antimicrobial properties of ZnO nanomaterials: A review. Ceram Int. 2017;43(5):3940-3961.
39. Ray Chowdhuri A, Tripathy S, Chandra S, Roy S, Sahu SK. A ZnO decorated chitosan–graphene oxide nanocomposite shows significantly enhanced antimicrobial activity with ROS generation. RSC Advances. 2015;5(61):49420-49428.
40. Suyana P, Nishanth Kumar S, Madhavan N, Dileep Kumar BS, Nair BN, Mohamed AP, et al. Reactive oxygen species (ROS) mediated enhanced anti-candidal activity of ZnS–ZnO nanocomposites with low inhibitory concentrations. RSC Advances. 2015;5(94):76718-76728.
41. Lallo da Silva B, Caetano BL, Chiari-Andréo BG, Pietro RCLR, Chiavacci LA. Increased antibacterial activity of ZnO nanoparticles: Influence of size and surface modification. Colloids Surf B Biointerfaces. 2019;177:440-447.
42. Tsogoo A. Synthesis, characterization and effect of doping on the photocoatalytic and antibacterial activities of zinc oxide: Agence Bibliographique de l'Enseignement Supérieur.
43. Chidhambaram N. Augmented antibacterial efficacies of the aluminium doped ZnO nanoparticles against four pathogenic bacteria. Materials Research Express. 2019;6(7):075061.
44. Schuler T, Aegerter MA. Optical, electrical and structural properties of sol gel ZnO:Al coatings. Thin Solid Films. 1999;351(1-2):125-131.
45. Elshikh M, Ahmed S, Funston S, Dunlop P, McGaw M, Marchant R, et al. Resazurin-based 96-well plate microdilution method for the determination of minimum inhibitory concentration of biosurfactants. Biotechnology Letters. 2016;38(6):1015-1019.
46. An Overview of the Clinical and Laboratory Standards Institute (CLSI) and Its Impact on Antimicrobial Susceptibility Tests. Antimicrobial Susceptibility Testing Protocols: CRC Press; 2007. p. 15-20.
47. At Gomes T, Gonzalez-Pedrajo B. Enteropathogenic Escherichia coli (EPEC). Pathogenic Escherichia coli in Latin America: BENTHAM SCIENCE PUBLISHERS; 2010. p. 25-47.
48. Razeghizadeh A, Mahmudi Ghalavandi M, Sohili F, Rafee V. The effect of sputtering RF power on structural, optical and electrical properties of CuO and CuO_2 thin films. Journal of Nanostructures. 2019; 9(2):230-237.
49. Razeghizadeh A, Elahi E, Rafee V. The effect of Mn doping on structural, magnetic and optical properties of TiO_2 nanoparticles. Journal of Nanoanalysis. 2018; 2(2):.77.
50. Razaghizadeh A.R, Elahi, E, Rafee V. Investigation of UV-Vis absorbance of TiO_2 thin films sensitized with the mulberry pigment cyanidin by sol-gel method. Nashrieh Shimi va Mohandesi Shimi Iran. 2016; 35(2): 1-8.